Wear 302 (2013) 1171–1179

Contents lists available at SciVerse ScienceDirect

Wear

journal homepage: www.elsevier.com/locate/wear

Wear mechanism and notch wear location prediction model in ball nose end milling of Inconel 718

M.S. Kasim [a,*], C.H. Che Haron [b], J.A. Ghani [b], M.A. Sulaiman [a], M.Z.A. Yazid [c]

[a] Department of Process, Faculty of Manufacturing Engineering, Universiti Teknikal Malaysia Melaka, Hang Tuah Jaya, Melaka, Malaysia
[b] Department of Mechanical and Material Engineering, Faculty of Engineering and Built Environment, Universiti Kebangsaan Malaysia, Bangi, Selangor, Malaysia
[c] Institute of Product Design and Manufacturing, UNIKL, Kuala Lumpur, Malaysia

ARTICLE INFO

Article history:
Received 4 September 2012
Received in revised form
18 December 2012
Accepted 22 December 2012
Available online 7 January 2013

Keywords:
Notch wear
Inconel 718
End milling
High-speed machining
Wear mechanism
Prediction model

ABSTRACT

This study is an investigation of tool wear using a ball-type end mill. The primary purpose of this work is to examine the tool life and wear mechanism when machining Inconel 718 with a physical vapor deposition (PVD)-coated carbide tool and varying the cutting parameters. Notch wear and flaking near the depth of the cut zone were the predominant types of tool failure for the four round cutting tools and were initiated by pitting caused by the repetitive cyclic load. The major factor identified was the large radial depth of the cut. Further examination indicated that the dominant wear was located near the depth of the cut line. On the flank face, smooth and coarse wear types, from abrasion and attrition, occurred at low and high cutting speeds, respectively. A maximum temperature of 521 °C was recorded, which is less than the critical temperature of 650 °C for Inconel 718. A mathematical model was developed to predict the location of the pitting, which was responsible for notching and flaking. This location could then be used to calculate the location associated with the maximum load exerted during the cutting. The error between the predictive model of pitting and the actual notching/flaking was less than 6%.

1. Introduction

Inconel 718 is well known as a material that is difficult to machine, even though it is widely used in high-temperature-environment components that require corrosion resistance, high strength, and ability to withstand creep rupture [1], e.g., in the aerospace industry, nuclear plants, and the biomedical industry [2,3].

Machining is generally difficult because of the toughness of the material and work hardening behavior. Most problems encountered during machining are caused by heat generation [4]. The low thermal conductivity of the material results in high cutting temperature, which is associated with deformation and friction at the tool-chip and tool-workpiece interface [5]. The problem occurs with Inconel 718 when cutting temperatures are below 650 °C, where the hardness of the material increases with increasing temperature [6]. Excessive strain during the ensuing machining passes creates undesirable microstructural alterations of the machined subsurface, causing work-hardening. This hardened surface layer increases the stress on the tool tip, making it sequential cuts extremely difficult [3]. The combination of applied stresses and temperatures causes flank wear and chipping [7]. Inconel 718 is 16, 6, and 4 times more difficult to machine than aluminum, mild steel, and stainless steel, respectively [8]. In machining materials that contain nickel, it is common to find that the notch wear has a significant effect on tool performance during end milling [7,9,10].

Welding and adhesion of the worked material onto the cutting tool, which frequently occur during machining, are the predominant factors causing severe notching and affecting the tool rake face from the consequent pull-out of coating and tool substrate [11]. Therefore, this material has been studied extensively for the analysis of tool life performance and surface integrity.

The life span of the cutting tool was determined from the tool wear, as a worn cutting tool may affect the surface quality. Therefore, predictive models are required to aid in selection of the appropriate process parameters. There are a large number of models related to machining processes, including the prominent Taylor equation for tool life, Archard and Usui's model of tool wear [12], and Altintas's model of cutting force [13]. These basic models have been extended to provide numerous other sophisticated models. Reliable models are necessary to minimize operational costs. However, in practice, some scenarios are difficult to model and require thorough investigation; tool life prediction is one such example. If the wear mechanism involves chipping and fracture rather than abrasion, the tool wear phenomenon is based on probability [14]. Current models have been aggressively developed by different approaches to meet the challenging requirements of today's competitive marketplace [15]; e.g., Quinsat predicted surface roughness by means of feed rate and tool tilt angle, [16]; D'addona, Leone, and Kaya developed tool wear prediction using ANN [17–19]; and Zhao investigated the effects

* Corresponding author. Tel.: +60 104642070; fax: +606 331 6411.
E-mail address: shahir@utem.edu.my (M.S. Kasim).

0043-1648/$ - see front matter © 2013 Elsevier B.V. All rights reserved.
http://dx.doi.org/10.1016/j.wear.2012.12.040

Nomenclature

ANN	Artificial neural network
BUE	Built up edge
DOC	Depth of cut
FEM	Finite element method
VB_1	Uniform flank wear
VB_3	Localized flank wear
V_c	Cutting speed
f_z	Feed rate
a_p	Axial depth of cut
a_e	Radial depth of cut
γ	Tangential angle
λ	Tool engagement angle
θ_{fmax}	Locating angle for maximum tangential force
θ_{init}	Locating entry angle
K	Maximum performance chip thickness
R_{eff}	Effective radius
θ_{doc}	Locating angle for depth of cut line
θ_{notch}	Locating angle for pitting area
t_{offset}	Insert offset from tool holder centerline
f_t	Tangential force

of internal cooling of the cutting tool to develop a flank wear model [20]. Fontaine studied the effect of surface inclination on the cutting force [21]. The effect of the stiffness of the cutting tool on tool wear was investigated by Takashi [22], and Shao developed a cutting power model to monitor tool wear in milling [23]. Taking advantage of computer technology, an FEM application was used to study cutting behavior and to estimate tool wear by Xie, Attanasio, and Ozel [24–26], and Nagi and Sivasakthivel predicted tool life by using a statistical method [27,28].

In milling, the cutting tool is subjected to a rubbing process, and the friction between the cutting tool and the workpiece generates heat [27]. For some operations, milling is an interrupted cutting process, and the wear mechanism is different from that in a continuous cutting process. In continuous cutting at low speed, BUE development is protects the rake face more stably than in the interrupted cutting process, where the tool life is one-tenth of that in continuous cutting [29]. An investigation by Krain et al. [30] reported that abrasion, adhesion and attrition were the main tool wear mechanisms, and a BUE is formed by high pressure and chemical affinity. This finding was supported by Sharman's work on end milling, which showed that BUE formation adheres to the cutting edge, some areas of the cutting tool possess bonds that are stronger than the coating-base material, and the repetitive plucking of the tool coating leads to exposure of the base material and consequent rapid wear of the tool [31]. The wear rate depends on the cutting temperature and the properties of the tool and workpiece material [32]. The wear rate stabilized when the temperature of localized heat was below 600 °C and accelerated when the temperature exceeded 680 °C [33]. Statistical analysis of the machining data revealed that over 80% of the tool performance was caused by the cutting variables of speed, feed rate, and depth of cut (DOC). Similar analysis showed that more than 98% of the tangential component of force is attributable to the influence of these same cutting variables. Cutting speed virtually dominated the wear rate, with DOC and feed rate jointly dominating the tangential component force [34]. In terms of tool geometry, a negative rake angle is preferable to prolong tool life, and a positive rake angle offers a better surface finish [35].

This study focuses on the pitting location. Pitting is the early stage of notch wear. It is based on the maximum force generated during tool rotation, and the mathematical prediction model was derived from the location of the maximum cutting force in conjunction with the maximum chip thickness.

2. Experimental set-up

In the cutting test, a CNC milling machining with a maximum speed of 8000 RPM was used for the experiment. The work material was a 160 mm × 100 mm × 50 mm block of aged, treated Inconel 718. The composition of the material is shown in Table 1. The block underwent a double aging process (Fig. 1.), where the raw Inconel was heated at 980 °C for 1 h, and then rapidly quenched in water, then reheated for 8 h at 720 °C, slowly cooled in the furnace until it reached 620 °C, then held at that temperature for 8 h. Finally, the block was cooled in open air [2,36,37].

The purpose of this aging treatment process is to convert AMS5662 grade (92 ± 2 HRB) to AMS 5663 grade (42 ± 2 HRC).

2.1. Cutting tool material

The cutting tool was a Sumitomo ball nose type milling cutter with a nominal diameter of 16 mm attached to a BIG Hi-Power Milling Chuck DV40-HMC20-85 for powerful and precise clamping. A tool overhang length of 60 mm was maintained throughout the experiment (Fig. 2). The insert was tungsten carbide with multi-layer PVD TiAlN/AlCrN grade ACK 300. The specifications of the cutting tool and tool holder used in this experiment are shown in Table 2.

2.2. Tool wear measurement and analysis

Tool wear was measured using a Mitutoyo toolmaker's microscope with 30× magnification and ±0.003 mm repeatability. To eliminate any influence of the previous cutting effect on the workpiece, each new layer was face-milled and cut into a block, with the last cut-out made using a non-test insert. After the specific pass interval, the cutting tool was removed from the tool

Table 1
Inconel 718 Composition.

Al	B	C	Cb.Ta	Co	Cr	Cu	Fe	Mn	Mo
0.49	0.004	0.051	5.05	0.30	18.30	0.04	18.70	0.23	3.05
Ni	P	S	Si	Ti					
53.0	< 0.005	< 0.002	0.08	1.05					

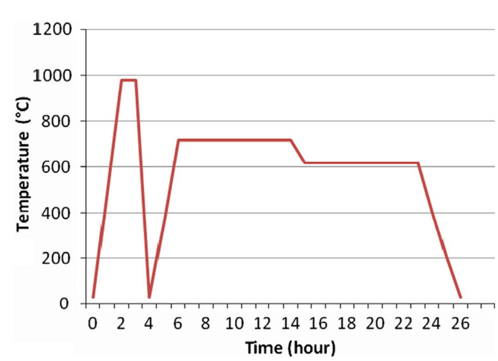

Fig. 1. Double aging schedule of Inconel 718 [2,36].

Fig. 2. Ball end mill used in the cutting test, attached to a high-power clamping chuck to improve rigidity.

Table 2
Cutting tool geometry.

Insert diameter, ∅	10 mm
Thickness	3.97 μm
Relief angle	11°
Radial rake angle	0°
Axial rake angle	−3°
Approach angle	90°
Number of inserts, n	1

holder to observe the progression of wear. Tests were stopped when tool failure occurred. In accordance with ISO 8688-2-1989 [38], tool life failure for an end mill is considered to occur when one of following criteria is met:

1. Uniform flank wear reaches 0.3 mm.
2. For irregular flank wear, the maximum wear is 0.5 mm.
3. Catastrophic failure.

The cutting parameters were set the same as the finishing process, and the variable parameters were cutting speed, feed rate, and radial and axial DOC. The fixed parameters were coating type and MQL flow rate. Details of the cutting conditions used in the experiment are shown in Table 3.

For further analysis, an NEC Thermo GEAR G100EX infrared thermal imager was used for temperature measurement with an emissivity setting of 0.17. Forces were measured using a Kistler model 5070 A dynamometer. The variable pressure scanning electron microscope (VPSEM) model Leo–Zeiss 1450 was used to capture the microscopic images of tool damage. This instrument was equipped with a Genesis 4000 XMS energy-dispersive x-ray spectroscopy (EDAX) system to analyze the element composition of selected cross-sectioned samples.

3. Results and discussion

Fig. 3 shows the growth of flank wear over cutting time. The wear trend was consistent with the pattern reported by others

Table 3
Cutting conditions.

Machine center	DMC 635 V Eco
Cutting tool	TiAlN/AlCrN, ACK 300 from Sumitomo
Nominal cutter diameter	16 mm
Workpiece material	Aged Inconel 718
Cutting speed	100–140 m/min
Feed rate, f_z	0.1–0.2 mm/tooth
Axial depth of cut, a_p	0.5–1.0 mm
Radial depth of cut, a_e	0.2–1.8 mm
Run out	10 μm (radial) and 5 μm (axial)
Overhang length	30 mm
Cutting configuration	Down milling
Lubricant	MQL with flow rate of 50 ml/h

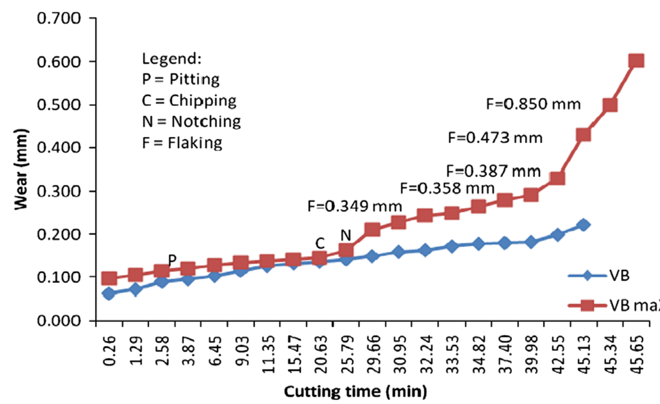

Fig. 3. Measured flank wear progression with other observed wear modes during the end milling of Inconel 718. V_c=140 m/min, f_z=0.15 mm/tooth, a_p=0.75 mm, a_e=0.2 mm.

[19,39,40]. Both uniform (VB) and localized flank wear (VB_3) were recorded. From the observations, at the initial stage of cutting time, the growth of flank wear increased steadily with increasing cutting length. The flank wear then grew unevenly and could be split into VB and VBmax when notching wear appeared. The highest peak in flank wear formed near the DOC line [5,41]. Notch wear initiated with pitting caused by the repetitive cyclic load. The pitting worsened, promoting the formation of chipping. This chipping accelerated the wear from notching while VB continued to follow a steady trend. Flaking occurred on the rake face due to the increase in cutting temperature, weakening the bonding between the coating and the base material [42].

Although the tool coating was removed, the cutting tool apparently withstood the cutting time. The final region was the critical zone, where the cutting tool approached the end of its tool life, and the notching and flaking sizes grew rapidly. In this region, the chip formation can change from elemental to continuous chipping (Fig. 4) because the chips weld together in notch wear during tool failure. The accumulated chips are then eliminated after several rotations. This phenomenon is a result of the higher cutting force and temperature caused by the rubbing between the stuck chips and the workpiece, which was demonstrated by the reddish color that appeared on the tool tip and the unpleasant audible noise produced. This propagation of flaking and notch wear subsequently caused catastrophic and unpredictable tool failure.

There is interest in the way that the diameter of the tool ball end affects the flank wear. At constant rotational speed, the cutting speed varies greatly for different tool diameters. Therefore, the flank wear can be divided into two types. Very smooth wear was observed at low cutting speeds near the tool tip region. Coarse wear appeared near the DOC line from the increased effective cutting speed arising from the round shape of the cutting tool. Fig. 5a shows an SEM image of flank wear along the cutting edge. The observed wear mechanisms were abrasion and attrition on the tool face and the cutting edge. The abrasive wear was caused by the rubbing action between the cutting tool and the workpiece. Inconel, which consists of carbide elements (CrC, TiC, MoC, WC, FeC and NbC) [43], removes tool material to create deep scratches and scores on the worn surface [31].

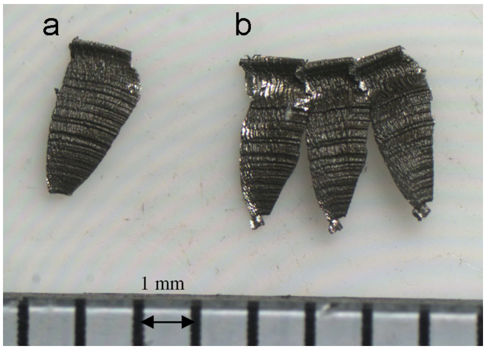

Fig. 4. Chip formation: (a) Elemental chip in good tool cutting condition (b) Accumulated chip in severe notch wear condition.

During end milling, a BUE intermittently occurred along the tool tip. At low effective cutting speeds, the chips welded to the cutting edge caused attrition when the small fragments of tool materials were dislodged as the BUE broke off (Fig. 5a) [44]. Near the DOC line, where the maximum chip thickness formed (Fig. 5b), the BUE occurred more aggressively because of higher stress acting on the cutting edge. A consequence of aggressive BUE break-off is the pitting problem, which occurs during interrupted machine operation and is typically found; a similar situation was reported by [30,31].

The pitting problem enlarges to form chipping (Fig. 6b). Chipping and abrasive wear increase to form notch wear (Fig. 6c), a groove that occurs at both the flank and rake faces of the cutting tool near the DOC line. Localized notch wear then leads to tool

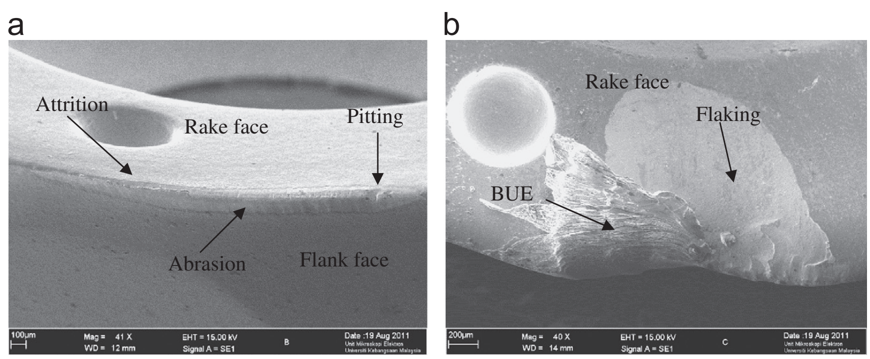

Fig. 5. Flank wear at initial stage of machining. BUE and flaking form on the rake face near the DOC line.

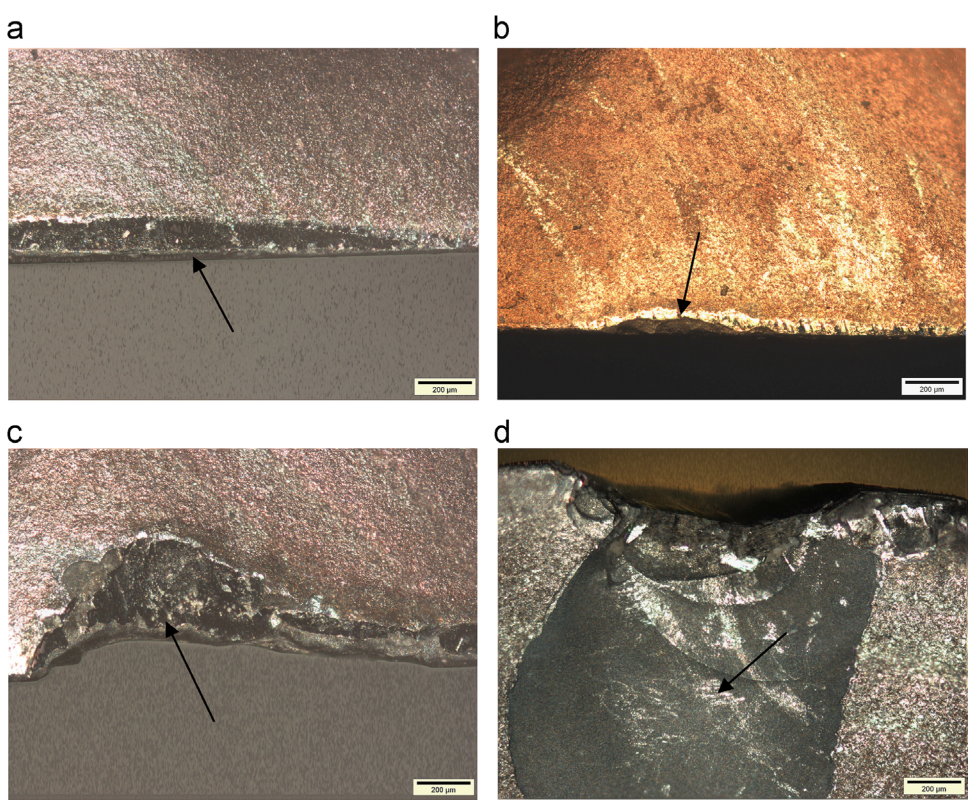

Fig. 6. Four common problem types when milling Inconel 718 with a round type TiAlN/AlCrN insert. (a) Flank wear, (b) Chipping, (c) Notch wear and (d) Flaking.

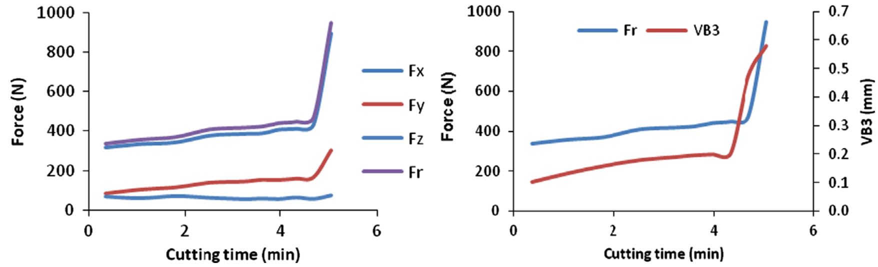

Fig. 7. Effect of tool wear on cutting force.

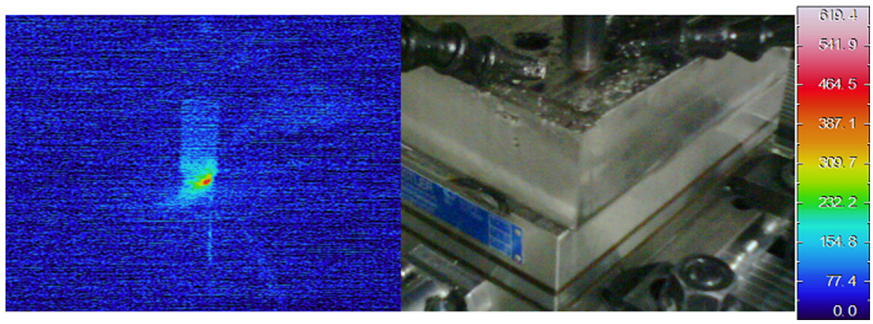

Fig. 8. Temperature recorded during end milling with a maximum temperature of 521 °C. The highest temperature was observed near the DOC line.

fracture. It was observed that the cutting forces were sensitive to the cutting condition; the cutting force increased with increasing notch wear [45] because of a change in the geometry during wear progression. Repetitive sudden impact on the cutting tool causes a flaking problem in which the coating breaks off (Fig. 6d), causing the cutting tool to fail catastrophically (Fig. 10) [46]. At that point, the cutting force increases sharply because of the loss of the cutting property. The progression of tool wear was recorded and is shown in Fig. 7.

In Fig. 8 the gradient of the temperature of the cutting tool near the vicinity of the DOC line can be observed, which corresponds to the highest contact area and friction between the cutting tool and the workpiece, as also observed by Lorentzon et al. [47]. Because the wear rate depends largely on the temperature, this location exhibits the most severe flank wear along the cutting edge. The rest of the cutting edge wear rate was relatively acceptable because of the effect of cooling and lubrication, which reduced the temperature at the cutting tool interface. The recorded temperature was 521 °C, which is below 650 °C, the critical temperature at which the Inconel material hardens as the temperature increases [6]. Therefore, wear appeared on the flank because of adhesive wear. Thermal wear would only occur above 680 °C [33].

Crater wear did not appear during machining because the temperature recorded was lower than the chemical dissolution temperature (1100 °C [8]) of the base material (WC), and diffusion wear was not observed during milling because the bonding strength between particles of carbide remained intact. Moreover, the chip flow was not on the rake face because of the cutting edge geometry, as shown in Fig. 9.

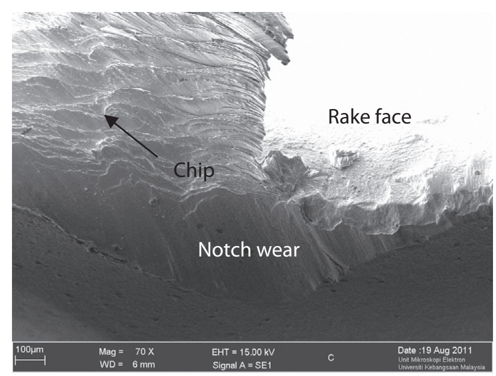

Fig. 9. Welded chip attached to the notched region of the cutting edge.

Fig. 10 shows the detail of the tool damage on the DOC line during catastrophic failure, which consists of abrasive wear on the flank and rake face, cavities that expose the base material, delamination of the TiAlN/ AlCrN coating, cracking, and a fracture that ruins the original shape.

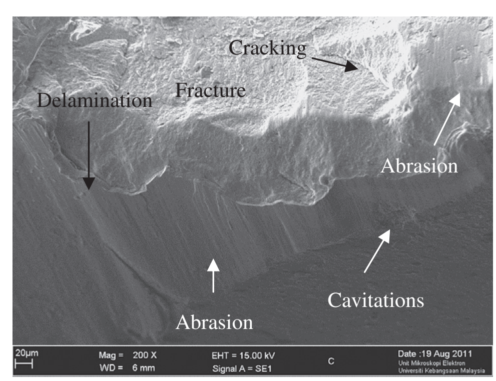

Fig. 10. Several failure modes during catastrophic failure.

Fig. 11a shows an SEM micrograph of the fractured cutting tool. The coating and base material were lost in the notching region (region A). The base material was covered with some adhering residual chips of the Inconel 718 material during chip flow. This observation was verified by the Ni, Cr and Fe elements revealed in spectrum A during EDAX analysis (Fig. 11b). A different behavior was observed in region B. Spectrum B (Fig. 11c) indicated that the coating (Ti, Al, Cr) remained. The flank face was the non-contacted surface during machining.

4. Development of the mathematical model

In general, the cutting force was exerted by the cutting tool in a system comprising three axes, X, Y, and Z. The resultant cutting force is a component of these three axes, resolved into geometrical and physical components [44]. In developing this model, the tangential force was selected because of the action of the force that is exerted perpendicular to the rake face plane (Fig. 11) [48].

The width of the radial DOC affects the tangential angle in conjunction with the tangential force [49]. The engaged angle was influenced by the combination of feed rate and radial DOC. During tool rotation, there was one point at which the cutting edge experienced the maximum load exerted onto the surface. This point was correlated with the thickness of the chip, which has been observed to vary with tool rotation [50] (Fig. 12).

To clarify the location during tool rotation, Deform3D simulation was used to identify the angle of maximum load after tool engagement. The cutting simulation showed that the maximum feed force occurs after the tool engages; the force rises sharply to a peak and gradually decreases as the chip volume decreases (Fig. 13). To validate the simulation, the effective cutting areas associated with tool motion were segregated into several segments, as shown in Fig. 14. These segments were cross-sectioned, revealing the tool-workpiece contact area for different cutter rotations. The area of contact varied along the cutter rotation [51]. The largest cutting engagement area, at the C–C′ angle, is the location of the maximum chip thickness and maximum load because the cutting force is proportional to the maximum chip area [49]. Fig. 14 shows the nomenclature of the tool engagement that experienced the maximum load. Fig. 16 shows a plane view, normal to the C–C′ axis.

Because the ball nose insert geometry is round, the effective radius is determined by the axial DOC. Therefore, the effective radius of the cutting tool can be obtained by Eq. (1) as follows:

$$\mathrm{r_{eff}} = \mathrm{t_{offset}} + \sqrt{\mathrm{r}^2 - (\mathrm{r} - \mathrm{ap})^2} \tag{1}$$

where r, a_p, and t_{offset} are the cutter radius, axial DOC, and tool offset, respectively. The location of the maximum contact area relative to the axial DOC is determined as follows:

$$\theta_{doc} = cos^{-1}\left(1 - \frac{ap}{r}\right) \tag{2}$$

Referring to Fig. 15, the entry angle, can be calculated as follows:

$$\theta_{init} = 180^\circ - cos^{-1}\left(1 - \frac{ae}{r_{aff}}\right) \tag{3}$$

During tool rotation, the angle at which the maximum force occurs, θ_{init}, is expressed by the use of Eqs. (1) and (3) as follows:

$$\theta_{f\ \max} = 180^\circ - \tan^{-1}\frac{r_{eff}\sin(180^\circ - \theta_{init}) - fz}{r_{eff} - ae} \tag{4}$$

Increasing the feed rate and radial DOC will increase the maximum chip thickness [49], K, whose value is given by the following relationship, which is a combination of Eqs. (1) and (4):

$$K = r_{eff} - \frac{r_{eff} - ae}{\cos(180^\circ - \theta_{f\ \max})} \tag{5}$$

Finally, the location of the predicted pitting can be worked out by Eqs. (2) and (5) as follows:

$$\theta_{notch} = tan^{-1}\left(r\frac{\sin\theta_{doc} - k/r}{1 - ap}\right) \pm e \tag{6}$$

5. Validation of the mathematical model

To validate the model, a comparison between pitting spots on the insert and the predicted location was performed with a total of 29 samples, shown in Table 4. The experimental variable parameters, including the insert size, were input into the predictive model. The model results agreed with the experiment results. The error in the observed results was 6%, which is relatively acceptable. There was a large deviation during narrow radial DOC. This deviation may be attributed to the low tangential force.

The relationship between the radial DOC and cutting force is shown in Fig. 16. The resultant force does not differ significantly

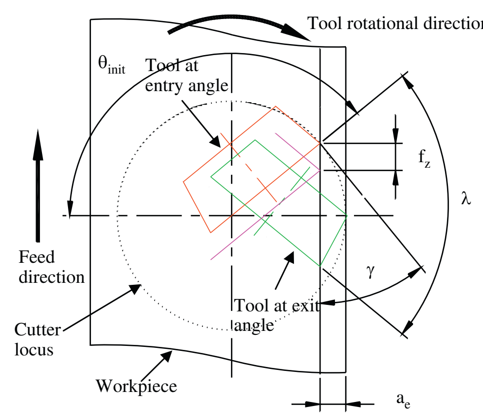

Fig. 12. Top view of peripheral milling indicates the nomenclature related to the development of the model.

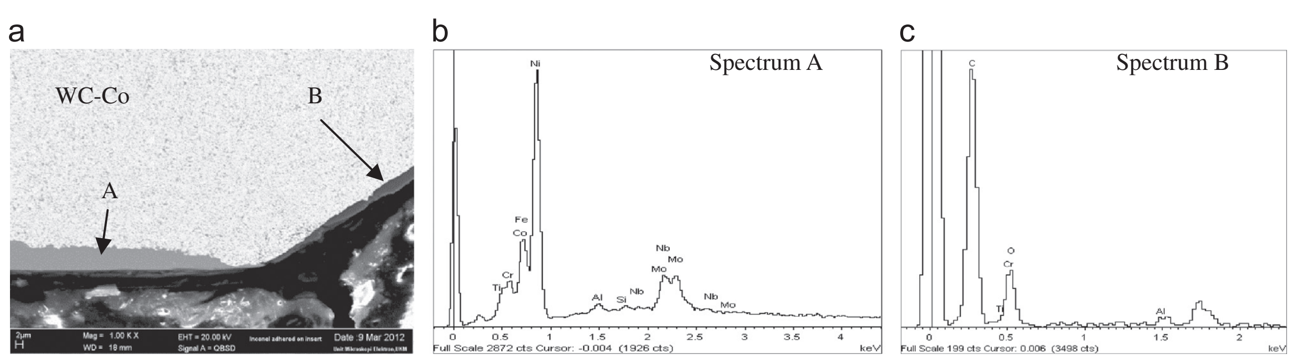

Fig. 11. (a) Cross section of PVD coated carbide at 9.46 min (V_c=120 m/min, f_z=0.15 mm/rev, a_p=0.75 mm, and a_e=1 mm). (b) EDAX analysis at the area of notch wear. (c) EDAX analysis at the flank face.

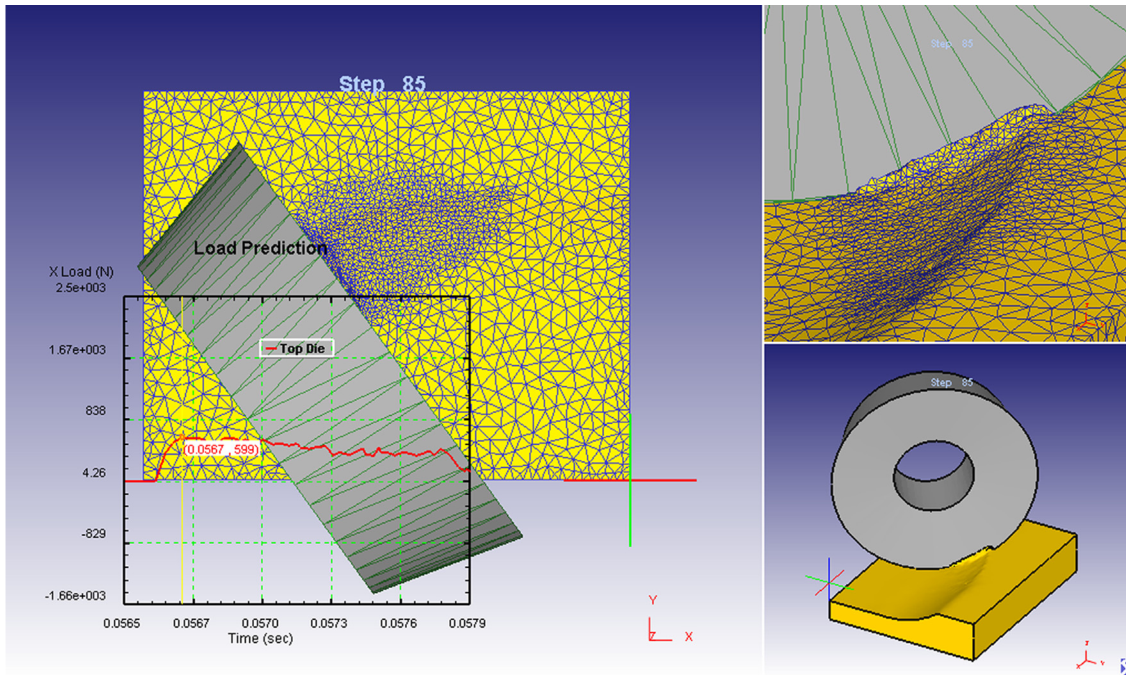

Fig. 13. Simulated chip formation during the cutting milling process indicates the peak of the cutting force that occurred in the moment after engagement with the workpiece. Cutting parameter of $V_c = 120$ m/min, $f_z = 0.2$ mm/tooth, $a_p = 1$ mm and $a_e = 1$ mm.

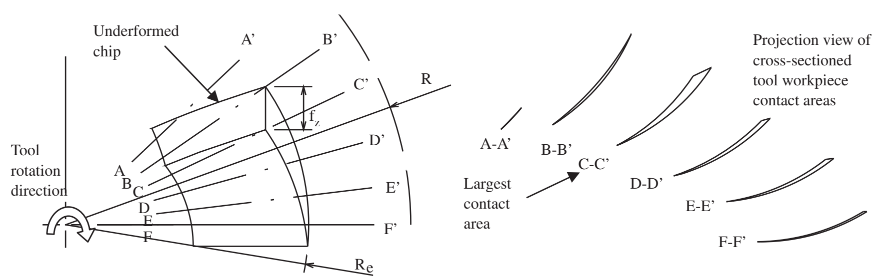

Fig. 14. Projection of uncut chip cross-section area for different effective cutter rotations.

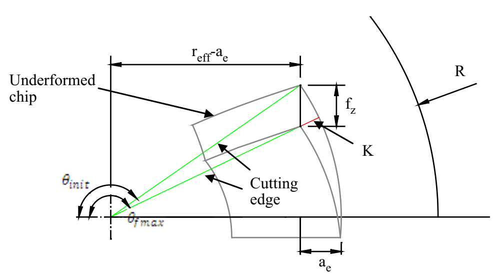

Fig. 15. Top view of preformed chip indicates the location of maximum force during tool rotation.

from the tangential force; consequently, it was neglected in this study [52]. Based on the calculation, the radial DOC corresponds to the tangential force. A wider radial DOC caused a smaller entry angle and larger tangential angle, and thus a higher tangential force was exerted on the cutting edge. The higher tangential force (F_t) was sufficient to plough the cutting edge at the DOC line to form pitting and chipping. While the smaller width of cut reduced the tangential force, the radial DOC of 0.2 mm increased the prevalence of abrasive wear over the impact of the tangential force in creating notch wear (Fig 17).

Fig. 18 shows an example of the error between the calculated and actual DOC line and pitting location. The actual pitting location occurred 30.98° from the tool tip compared to the calculated value of 30.71° (0.8% error), and the actual DOC location occurred 32.29° from the tool tip, whereas the calculated location was 31.79° (1.5%). The error varied according to the width of cut. A wider radial DOC normally causes a larger tangential force due to the small entry angle; a narrow radial DOC causes a small tangential force because of the wider entry angle. A tangential force below 200 N gave a larger error of 2.8%, while the error for a tangential force between 201 and 300 N was 1.4%, and that for a tangential force greater than 300 N was found to be below 0.9% (Fig. 19).

6. Conclusions

Notch wear is the predominant failure mode during end milling of Inconel 718. This wear is typically located near the DOC line when machining a nickel-based alloy. Two components that affected notch wear are the radial DOC and the cutting speed. The radial DOC affects the volume of material, and the cutting speed affects the cutting temperature. As notch wear increases, the cutting force and temperature increase. Flaking occurred at the rake face because of the thermal load there. Flaking and notch wear propagation were more aggressive in the rapid segment of the wear curve. Ultimately, the combination of notch wear and flaking caused the cutting edge to fail abruptly.

Table 4
Comparison of pitting location near DOC line.

Run Test no.	V_c (m/min)	f_z (mm/tooth)	a_p (mm)	a_e (mm)	Calculated pitting location (°)	Observed pitting location (°)	Error (°)
1	100	0.15	0.75	0.2	31.42	32.21	0.79
2	120	0.15	1	0.2	36.53	35.93	−0.60
3	120	0.1	1	1	36.37	34.77	−1.60
4	120	0.15	0.75	1	30.96	30.31	−0.65
5	100	0.15	0.75	1.8	30.71	30.97	0.26
6	120	0.15	0.5	0.2	25.44	15.74	−9.70
7	140	0.15	0.75	0.2	31.42	31.63	0.21
8	120	0.2	0.5	1	24.64	23.28	−1.36
9	120	0.2	0.75	0.2	31.30	30.87	−0.43
10	120	0.15	0.75	1	30.96	30.42	−0.54
11	120	0.1	0.75	0.2	31.54	30.88	−0.66
12	120	0.1	0.5	1	25.24	21.67	−3.57
13	140	0.15	0.75	1.8	30.71	29.86	−0.85
14	120	0.15	0.75	1	30.96	30.10	−0.86
15	120	0.1	0.75	1.8	31.07	30.08	−0.99
16	120	0.2	0.75	1.8	30.36	32.15	1.79
17	100	0.2	0.75	1	30.69	31.80	1.11
18	140	0.15	0.5	1	24.94	19.80	−5.14
19	120	0.15	0.5	1.8	24.67	23.37	−1.30
20	120	0.15	1	1.8	35.88	34.54	−1.34
21	100	0.15	0.5	1	24.94	23.94	−1.00
22	140	0.15	1	1	36.11	35.65	−0.46
23	100	0.1	0.75	1	31.24	31.13	−0.11
24	140	0.1	0.75	1	31.24	31.71	0.47
25	120	0.2	1	1	35.87	35.60	−0.27
26	100	0.15	1	1	36.11	36.70	0.59
27	140	0.2	0.75	1	30.69	29.13	−1.56
28	120	0.15	0.75	1	30.96	30.76	−0.20
29	120	0.15	0.75	1	30.96	29.84	−1.12

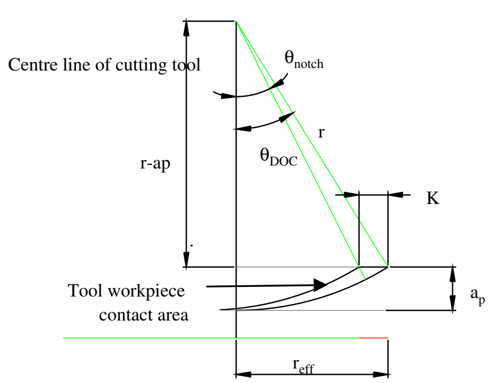

Fig. 16. Plane view of (C–C′) cross-section (maximum tool contact area) indicating nomenclature associated with Eqs. (1) and (2).

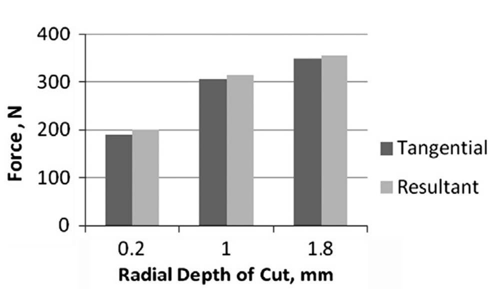

Fig. 17. Effect of radial DOC on tangential and resultant forces.

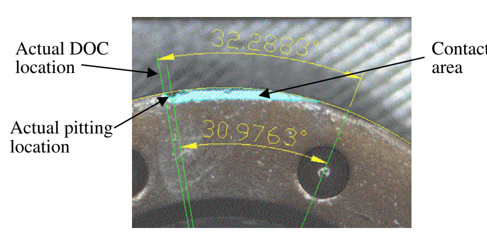

Fig. 18. Test no. 5, calculated pitting location of 30.71° (0.8%) and DOC line of 31.79° (1.5%). V_c=100 m/min, f_z=0.15 mm/tooth, a_p=75 mm, a_e=1.8 mm, F_t=340 N.

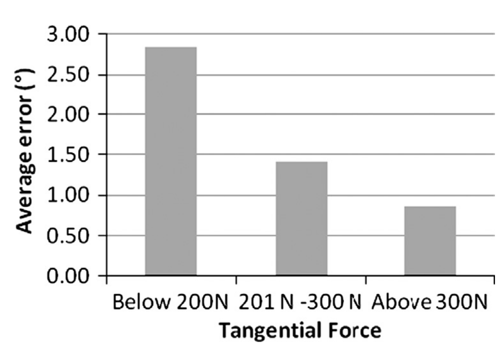

Fig. 19. Effect of tangential force on calculation error.

A predictive model for notch wear location in ball nose end milling of Inconel 718 has been successfully developed. The model equation considers the cutting condition, feed rate, axial and radial DOC, and tool size. It was able to predict the pitting location on the cutting edge, which is the initial stage in developing notch wear. Validation was performed with 29 samples, and the results predicted by the model were compared against actual data. The average errors are relatively acceptable, with 6% deviation.

Acknowledgments

The authors wish to thank Universiti Teknikal Malaysia Melaka, the CRIM Division of Universiti Kebangsaan Malaysia for the Thermal Imager, and the Government of Malaysia for technical and financial support for the experiment. This research was supported by the Higher Education Ministry of Malaysia through project no. UKM-GUP-BTT-07-25-171.

References

[1] T. Kitagawa, A. Kubo, K. Maekawa, Temperature and wear of cutting tools in high-speed machining of Inconel 718 and Ti6Al6V2Sn, Wear 202 (1997) 142–148.
[2] I.A. Choudhury, M.A. El-Baradie, Machinability of nickel-base super alloys: a general review, Journal of Materials Processing Technology 77 (1998) 278–284.
[3] D. Ulutan, T. Ozel, Machining induced surface integrity in titanium and nickel alloys: A review, International Journal of Machine Tools & Manufacture 51 (2011) 31.
[4] M.C. Shaw, Metal Cutting Principles, 2nd Ed, Oxford University Press, New York, 2005, ed.
[5] E.O. Ezugwu, Key improvements in the machining of difficult-to-cut aerospace superalloys, International Journal of Machine Tools and Manufacture 45 (2005) 1353–1367.
[6] Y.S. Liao, H.M. Lin, J.H. Wang, Behaviors of end milling Inconel 718 superalloy by cemented carbide tools, Journal of Materials Processing Technology 201 (2008) 460–465.
[7] E.O. Ezugwu, Z.M. Wang, A.R. Machado, The machinability of nickel-based alloys: a review, Journal of Materials Processing Technology 86 (1999) 1–16.
[8] E.E. O, Key improvements in the machining of difficult-to-cut aerospace superalloys, International Journal of Machine Tools and Manufacture 45 (2005) 1353–1367.
[9] M. Rahman, W.K.H. Seah, T.T. Teo, The machinability of inconel 718, Journal of Materials Processing Technology 63 (1997) 199–204.
[10] R.T. Coelho, L.R. Silva, A. Braghini, A.A. Bezerra, Some effects of cutting edge preparation and geometric modifications when turning Inconel 718(TM) at high cutting speeds, Journal of Materials Processing Technology 148 (2004) 147–153.
[11] L. Li, N. He, M. Wang, Z.G. Wang, High speed cutting of inconel 718 with coated carbide and ceramic inserts, Journal of Materials Processing Technology 129 (2002) 127–130.
[12] E. Usui, T. Shirakashi, T. Kitagawa, Analytical prediction of cutting tool wear, Wear 100 (1984) 129–151.
[13] Y. Altintas, P. Lee, A general mechanics and dynamics model for helical end mills, CIRP Annals - Manufacturing Technology 45 (1996) 59–64.
[14] T. Childs, K. Maekawa, T. Obikawa, Y. Yamane, Metal Machining; Theory abd Applications, John Wiley & Sons Inc., New York, 2000.
[15] V.P. Astakhov, An opening historical note, International Journal of Machining and Machinability of Materials 1 (2006) 3–11.
[16] Y. Quinsat, S. Lavernhe, C. Lartigue, Characterization of 3D surface topography in 5-axis milling, Wear 271 (2011) 590–595.
[17] D. D'Addona, T. Segreto, A. Simeone, R. Teti, ANN tool wear modelling in the machining of nickel superalloy industrial products, CIRP Journal of Manufacturing Science and Technology 4 (2011) 33–37.
[18] C. Leone, D. D'Addona, R. Teti, Tool wear modelling through regression analysis and intelligent methods for nickel base alloy machining, CIRP Journal of Manufacturing Science and Technology 4 (3) (2011) 327–331.
[19] B. Kaya, C. Oysu, H.M. Ertunc, Force-torque based on-line tool wear estimation system for CNC milling of inconel 718 using neural networks, Advances in Engineering Software 42 (2011) 76–84.
[20] H. Zhao, G.C. Barber, Q. Zou, A study of flank wear in orthogonal cutting with internal cooling, Wear 253 (2002) 957–962.
[21] M. Fontaine, A. Moufki, A. Devillez, D. Dudzinski, Modelling of cutting forces in ball-end milling with tool-surface inclination: Part I: Predictive force model and experimental validation, Journal of Materials Processing Technology 189 (2007) 73–84.
[22] T. Miyaguchi, M. Masuda, E. Takeoka, H. Iwabe, Effect of tool stiffness upon tool wear in high spindle speed milling using small ball end mill, Precision Engineering 25 (2001) 145–154.
[23] H. Shao, H.L. Wang, X.M. Zhao, A cutting power model for tool wear monitoring in milling, International Journal of Machine Tools and Manufacture 44 (2004) 1503–1509.
[24] L.J. Xie, J. Schmidt, C. Schmidt, F. Biesinger, 2D FEM estimate of tool wear in turning operation, Wear 258 (2005) 1479–1490.
[25] T. Özel, M. Sima, Finite element simulation of high speed machining Ti-6Al-4V alloy using modified material models, in: Proceedings of the 38th North American Manufacturing Research Conference (NAMRC), Society of Manufacturing Engineers, Queen's University, Kingston, Ontario, Canada., 2010, pp. 49–56.
[26] A. Attanasio, E. Ceretti, A. Fiorentino, C. Cappellini, C. Giardini, Investigation and FEM-based simulation of tool wear in turning operations with uncoated carbide tools, Wear 269 (2010) 344–350.
[27] P.S. Sivasakthivel, V.V. Murugan, R. Sudhakaran, Prediction of tool wear from machining parameters by response surface methodology in end milling, International Journal of Engineering Science and Technology 2 (2010) 1780–1789.
[28] N.H. Elmagrabi, F.M. Shuaeib, C.H.C. Haron, An overview on the cutting tool factors in machinability assessment, Journal of Achievements in Materials and Manufacturing Engineering 23 (2007) 87–90.
[29] K. Yamamoto, M. Kuroda, H. Omokawa, K. Itakura, High-Efficiency Cutting of Super-Heat-Resistant Alloy, Mistubishi Heavy Industry, Ltd, available from 〈http://www.mhi.co.jp/en/technology/review/indexe-38-1.html〉 (accessed 1 38).
[30] H.R. Krain, A.R.C. Sharman, K. Ridgway, Optimisation of tool life and productivity when end milling Inconel 718TM, Journal of Materials Processing Technology 189 (2007) 153–161.
[31] A. Sharman, R.C. Dewes, D.K. Aspinwall, Tool life when high speed ball nose end milling Inconel 718, Journal of Materials Processing Technology 118 (2001) 29–35.
[32] B.M. Kramer, V.T. B.F., A Comprehensive tool wear model, CIRP Annals—M anufacturing Technology 35 (1986) 67–70.
[33] S. Katsuhiko, Y. Yasuo, N. Norihiko, Tool wear under high speed end milling of nickel-base superalloy inconel 718, Journal of the Japan Society for Precision Engineering 70 (2004) 1086–1090.
[34] E.O. Ezugwu, K.A. Olajire, Z.M. Wang, Wear analysis of coated carbide tools when machining nickel base, Inconel 718 Alloy, in: Surface Modification Technologies XIV: Proceedings of the Fourteenth International Conference on Surface Modification Technologies 2000 ASM International, Montreal, 2000, pp. 279–286.
[35] B. Winegard, The positive and negative of cutting tool geometries, Seco, available from 〈www.secotool.com/us〉 (accessed 18.06.12).
[36] C.M. Kuo, Y.T. Yang, H.Y. Bor, C.N. Wei, C.C. Tai, Aging effects on the microstructure and creep behavior of Inconel 718 superalloy, Materials Science and Engineering: A 510–511 (2009) 289–294.
[37] N.S. Alloys, 718 Inconel® Nickel Alloy Bar, National Specialty Alloys, available from http://www.nsalloys.com/718-nickel-alloy-bar.html (accessed 3.03.11).
[38] ISO8688-2, Tool Life Testing in Milling—Part 2: End Milling, International Organization for Standardization, Geneva, 1989.
[39] C.H.C. Haron, A. Ginting, H. Arshad, Performance of alloyed uncoated and CVD-coated carbide tools in dry milling of titanium alloy Ti-6242S, Journal of Materials Processing Technology 185 (2007) 77–82.
[40] M. Alauddin, M.A. El Baradie, M.S.J. Hashmi, Tool-life testing in the end milling of Inconel 718, Journal of Materials Processing Technology 55 (1995) 321–330.
[41] E.O. Ezugwu, J. Bonney, D.A Fadare, W.F. Sales, Machining of nickel-base, Inconel 718, alloy with ceramic tools under finishing conditions with various coolant supply pressures, Journal of Materials Processing Technology 162-163 (2005) 609–614.
[42] A. Jawaid, S. Koksal, S. Sharif, Cutting performance and wear characteristics of PVD coated and uncoated carbide tools in face milling Inconel 718 aerospace alloy, Journal of Materials Processing Technology 116 (2001) 2–9.
[43] E. Bradley, Superalloy: A Technical Guide, ASM International, Metal Park, 1989.
[44] W. Grzesik, Advanced Machining Processed of Metallic Materials; Theory, Modelling and Applications, 1st Ed ed., Oxford, 2008.
[45] H.Z. Li, H. Zeng, X.Q. Chen, An experimental study of tool wear and cutting force variation in the end milling of Inconel 718 with coated carbide inserts, Journal of Materials Processing Technology 180 (2006) 296–304.
[46] H.A. Abdel-Aal, M. Nouari, M.E. Mansori, The effect of thermal property degradation on wear of WC–CO inserts in dry cutting, Wear 265 (2008) 1670–1679.
[47] J. Lorentzon, N. Järvstråt, B.L. Josefson, Modelling chip formation of alloy 718, Journal of Materials Processing Technology 209 (2009) 4645–4653.
[48] M. Alauddin, M.A. El Baradie, M.S.J. Hashmi, Modelling of cutting force in end milling Inconel 718, Journal of Materials Processing Technology 58 (1996) 100–108.
[49] W.H. Lai, Modeling of Cutting Forces in End Milling Operations, Tamkang Journal of Science and Engineering 3 (2000) 15–22.
[50] Y. Sun, F. Ren, D. Guo, Z. Jia, Estimation and experimental validation of cutting forces in ball-end milling of sculptured surfaces, International Journal of Machine Tools and Manufacture 49 (2009) 1238–1244.
[51] E. Pay, M. Cosma, Vertical path strategy for 3D CAD analysis of chip area in 3 axes ball nose end milling, in: Proceedings of the International multidisciplinary conference, 7th, Baia Mare, Romania, 2007, pp. 115–120.
[52] L. Ning, S.C. Veldhuis, K. Yamamoto, Investigation of wear behavior and chip formation for cutting tools with nano-multilayered TiAlCrN/NbN PVD coating, International Journal of Machine Tools and Manufacture 48 (2008) 656–665.